Particle retention in a submerged meadow and its variation near the leading edge

Elizabeth Follett*, Heidi Nepf

Department of Civil and Environmental Engineering, Massachusetts Institute of Technology, 77 Massachusetts Avenue Room 1-290, Cambridge, MA, 02139, USA

E-mail: emf@alum.mit.edu, hmnepf@mit.edu

*Corresponding author: Tel.: +1 (847) 471-8878, Fax: +1 (817) 258-8850

Abstract

The retention of particles within meadows of submerged aquatic vegetation impacts the fate of organic matter, pollen, and larvae. Because flow conditions near the leading edge differ from those over the bulk of the canopy, particle retention is likely to differ as well. In particular, near the leading edge of a wide meadow, flow deceleration generates a vertical updraft, which impacts particle fate. In the fully developed region of the meadow, shear-layer vortices at the top of the meadow may also influence particle fate. In this study the retention of particles was measured along the length of a 10-m model meadow (height 0.1m), and was connected to the evolving flow field. Two particle sizes, with settling velocity m s^{-1}, were released at two heights within the model meadow — The retention of particles was measured using microscope slides distributed along the flume bed. Retention increased with distance from the leading edge, associated with the decrease in vertical updraft. Retention was also greater for the particles with higher settling velocity. In the fully developed region of the meadow, particle retention was lower for particles influenced by the shear-layer vortices at the top of the meadow (—).

Keywords: particle transport, leading edge, capture, initial adjustment region, velocity ratio

Introduction

Submerged aquatic vegetation, such as seagrasses, are foundational species of coastal habitats (Green and Short 2003). Dense meadows stabilize sediment, lowering turbidity and sequestering carbon stocks, and increase biodiversity by providing sheltered regions (Waycott et al. 2009, Marbà et al. 2015; van Katwijk et al. 2016). The presence of seagrass meadows is associated with a reduction in coral disease levels and reduced amounts of coral pathogens, many of which are sediment-associated (Lamb et al. 2017). Suspended particles respond to the flow structure within and around submerged vegetation, creating distinct patterns of deposition that influence future meadow growth and resilience (Sand-Jensen 1998; Hughes and Stachowicz 2004; van Katwijk et al. 2016). Dense seagrass meadows have been observed to increase sedimentation and reduce resuspension relative to bare bed regions (Ward et al. 1984; Gacia et al. 1999; Terrados and Duarte 2000; Gacia and Duarte 2001; Agawin and Duarte 2002) while erosion and resuspension have been observed in sparse meadows (Luhar et al. 2008; van Katwijk et al. 2010; Lawson et al. 2012). Enhanced fine particle deposition has also been observed in the wake of finite patches of vegetation (Gurnell et al. 2001; Tanaka and Yagisawa 2010; Chen et al. 2012), while diminished deposition has been observed near the leading edge of emergent canopies (Zong and Nepf 2010). In this paper we consider the retention of particles released in a long, submerged model meadow comprised of rigid rods, making connections between the observed deposition and the flow structure at the leading edge and in the fully-developed region of the model meadow. Rigid rods were used to allow capture of particles on slides without the interference of flexible blades, which fall to the flume bed after water is drained from the flume. The flow diversion and canopy shear layer that develop over a rigid canopy is similar to that over a flexible canopy, so that a rigid canopy mimic appropriately captures relevant canopy-scale flow dynamics, although the coherent structures that develop in the shear layer are slightly stronger for a rigid canopy (Ghisalberti and Nepf 2006).

Flow evolution over a submerged meadow is depicted in Figure 1. The streamwise and vertical coordinates are ( ) and the corresponding velocity vector is , with at the leading edge and at the bed, and positive in the upward direction. Current entering the meadow at the leading edge is decelerated over a distance called the adjustment length (Chen et al. 2013). In a meadow with width ( ) much greater than its height ( ), this deceleration triggers a vertical updraft that has a maximum at the leading edge ( ) and decays

exponentially over the adjustment length-scale, (Belcher et al. 2003; Chen et al. 2013). The adjustment length, , scales with the canopy drag length scale (Belcher et al. 2003):

——— (1)

in which is the canopy solid volume fraction, is the canopy drag coefficient, and is the frontal area per canopy volume. The adjustment length is

— (2)

with scale factors and determined from a range of terrestrial and aquatic canopies with submergence ratios 2 to (Chen et al. 2013). A shear-layer profile begins to take shape within the adjustment region, as flow above the canopy accelerates and flow within the canopy decelerates. However, the development of shear-layer coherent structures at the top of the canopy (Raupach et al. 1996; Ghisalberti and Nepf 2002) is constrained within the adjustment region by the vertical updraft (Irvine et al. 1997; Morse et al. 2002). Beyond , the shear-layer structures develop and grow with distance from the leading edge, eventually reaching a constant size and strength at a distance (Ghisalberti and Nepf 2002, 2004; Chen et al. 2013). Beyond , the mixing layer is considered fully developed, at which point the shear velocity at the top of the meadow becomes constant, and shear-layer vortices penetrate into the canopy a distance Nepf et al. 2007). Turbulence in the upper canopy is dominated by shear-layer vortices, which have velocity scale . In the lower canopy , below the penetration of the shear-layer vortices, turbulence may be locally generated in the wakes of individual shoots, if Reynolds number (ud_s/ν) based on shoot diameter, d_s, is greater than about 100 (Nepf and Vivoni 2000; Liu and Nepf 2016).

In this study we measured the retention of particles within the leading edge and fully developed region of a 10-m long model canopy composed of rigid dowels, making connections to the leading edge and fully developed flow structure described above. Particles were injected at different longitudinal locations to assess how the evolving velocity field impacted particle retention at particular locations within the canopy.

Methods

Experiments were conducted using a rigid, model canopy that was 10 m long, m tall and spanned the width (m) of a recirculating flume (September 2013 – January 2016). The model canopy was constructed of circular wooden rods (rods cm^{-2}, m^{-1}, cm) placed in a staggered formation, with spacing 3.2 cm in the direction (normal to the flow) and 3.7 cm in the direction (along the main flow direction). The canopy height and density were chosen so that canopy scale vortices penetrated approximately half the canopy height. Using , 0.43, allowing investigation of the effects of canopy flow structure on particle fate. The canopy solid volume fraction was – = 0.027.

Three components of velocity were recorded using an acoustic Doppler velocimeter (ADV, Nortek Vectrino). Each record was collected for 4 min at 25 Hz. Silica seeding particles (Sphericel 110P8, Potters Industries, Malvern, Pennsylvania) were added to the water to enhance the ADV signal. Longitudinal transects at 10-cm intervals were made at and at three vertical positions: above (0.81, 1) and below (0.31) the penetration distance of the canopy scale vortices, 0.43. In addition, a lateral profile was recorded within the fully developed region . For each measurement the ADV was centered between the staggered dowels in such a way that the longitudinal velocity, vertical velocity, and Reynolds stresses were close to the lateral average value over the element spacing (as described by Chen et al. 2013, Fig. 2d in that paper). The velocity records were decomposed into time-average and fluctuating components ( ), respectively denoted by an overbar and prime. The Reynolds stress ( ) was found by multiplying and subsequently time-averaging the vertical and longitudinal fluctuations. Turbulent kinetic energy was calculated as – . The friction velocity at the top of the canopy was defined as $\overline{\quad}$.

A series of particle releases were conducted at two heights: within the upper canopy, where particles were impacted by canopy-scale vortices ( ) and below the penetration of the canopy scale vortices ( ). Two sizes of silica particles (Potters Industries, Malvern, Pennsylvania) were released inside the canopy and deposited on glass microscope slides. The particle size distribution was measured using laser diffraction (Beckman Coulter, Table 1). For the smaller particles, the settling velocity was found using Stokes' law (

———————), with 2500 kg m^{-3}, = 1000 kg m^{-3}, 8.9e-4 kg m^{-1} s^{-1}, and *d* the particle diameter. The larger particles did not satisfy the condition for Stokes flow (———). The settling velocity of the larger particles was found by using an approximation for valid for this intermediate regime (Denn 1980, Eq. 4.12). The particle sizes and channel velocity were chosen to create specific transport regimes. The larger particles (Spheriglass A2024, m s^{-1}) were chosen to have a median settling velocity, , comparable to the shear velocity at the top of the canopy (= 0.013 m s^{-1}, = 1.4), so that shear-layer turbulence would have only a weak influence on settling. The smaller particles (Spheriglass E3000, m s^{-1}) were chosen to have (= 0.06), so that particle transport would be strongly influenced by canopy turbulence. It is useful to relate these two regimes to typical field conditions, for which the velocity at the top ( ) of a meadow might be from 10–100 cm s^{-1}, for which we estimate 3.8–38 cm s^{-1} (Ghisalberti 2009). Assuming a sediment density equal to quartz (kg m^{-3}) and spherical sediment grains, the lighter particles tested in these experiments would correspond to sediment sizes 50 μm – 0.15 mm (silt-medium sand), and the heavier particles used would correspond to sediment sizes of 0.3–0.8 mm (medium-coarse sand).

Particles were injected into the canopy at different longitudinal locations within the leading edge and the fully developed region (0, 2.4, 5, 13.7, 53.3). Before the experiment, 60 glass microscope slides (2.5 cm x 7.5 cm were labeled and weighed. The slides (oriented with long side perpendicular to the mean flow) were placed in rows with centers at , and with rows at 20 streamwise locations. The rows were concentrated immediately downstream of the injection location, as shown in Figure 2, but also with several rows upstream and farther downstream for reference (not shown in Figure 2). Silica particles were mixed with water to form a dilute solution (E3000: 175 g silica in 10 L water; A2024: 75 g silica in 10 L water). A smaller mass of A2024 was released to prevent losses due to particles rolling off the slides, which occurred when larger initial masses were used. The particle/water solution was continually mixed in a 19-L plastic bucket and injected through a 2-mm nozzle into the flume using a peristaltic pump (Manostat Preston, Barrington, Illinois). The injection took one hour, which was long compared to the timescale of the shear-layer vortices (10 s) and the flume recirculation time (5 min). The tubing was taped to a rigid rod inside the flume and attached to a two-way nozzle pointing in the directions, to enhance lateral spreading. After injection, the flume was slowly drained and the slides were allowed to dry for

several days. After the initial drying period, the slides were removed from the flume using tweezers. Slides with heavy deposition were placed in aluminum boats to reduce particle loss. The slides were dried in a 50˚C drying oven (VWR) for one day. After drying, the slides were reweighed and the difference in weights was assumed to be entirely due to the settled particles. Two blank experiments measuring the change in slide weight with no particles released determined that there was a negligible amount of other material in the flume water,

(SD).

In order to estimate the total deposition within the model canopy, it was necessary to extrapolate values of deposition between the slides and the flume walls (cm, cm). Based on visual inspection after the flume was drained and dried, the particle deposition was concentrated near the center of the flume. Particle deposition extended to the walls for the E3000 particles, and was zero at the walls for the larger A2024 particles. Based on this, the deposition of E3000 particles between the outermost slides and the sidewalls was assumed to be the average of the outermost slides, and deposition of A2024 particles was assumed to decrease linearly from the deposition measured on the outermost slides to 0 at the walls. The fraction of particles released that deposited within the canopy was calculated as

—— (3)

Where is the total mass of particles added to the slurry, is the measured deposition cm^{-2} on an individual slide and is the average deposition cm^{-2} on all slides upstream of the injection site, representing deposition associated with recirculated particles. Deposition within the region covered by each slide was assigned to the measured deposition for that slide, and linear interpolation was used to estimate deposition outside the region covered by the slides. The integration in (3) was approximated by trapezoidal sums. In order to evaluate uncertainty, replicate experiments were conducted for four releases (see Table 2). The difference between replicate experiments was greater than the uncertainty from the standard error on , so replicate error was used as the estimate of uncertainty.

Results

The velocity measurements were used to evaluate the length of the adjustment region, , and the distance to the fully developed region, , which we used to select release locations. Time-mean longitudinal ( ) and vertical ( ) velocity decreased with distance from the leading edge (, Fig. 3 a,b). Based on the drag length scale (m^{-1}, eq. 1, assuming = 1), we expected the adjustment region to end at (eq. 2), which is denoted with a black vertical line in Figure 3. Consistent with this, the vertical velocity had decayed to zero by this point (Fig. 3b). Within the adjustment region ( ), Reynolds stress remained small (Figure 3c), but began to increase beyond , indicating development of the shear layer and associated vortices. Reynolds stress reached a constant value in the fully developed region ( ). The fully-developed shear velocity at the top of the canopy (0.013 m s^{-1}) was estimated from a lateral transect made in the fully developed region. In the fully developed region (30) turbulent stresses measured in the upper canopy (0.81 and 1) were much higher than those measured in the lower canopy (0.31), reflecting limited penetration of turbulence into the canopy, and specifically that shear-layer vortices did not penetrate to the lower canopy.

Particles were released within the adjustment region near the leading edge (, and within the fully developed region . Releases were conducted at two heights , above and below the vortex penetration distance — . The shape and size of the deposition region changed across the adjustment region, due to the influence of the vertical updraft. For the releases at (Fig. 4a,b), 98% of the particles had a settling velocity less than the updraft at the release point (m s^{-1}, at 0.81 and 0.31, respectively). For these releases the location of maximum deposition did not occur immediately after the release point, but at cm and cm downstream (for 0.81, 0.31, respectively), because particles were initially carried upward by the updraft, and settled after the updraft had decayed. As the release point moved farther from the leading edge, the updraft at the release point decreased (Figure 3b and Table 2), and as a result the distance between the point of release and the location of maximum deposition, , also decreased (Table 2).

As the updraft decayed with distance from the leading edge, the shape of the deposition mound changed; peak deposition increased and the streamwise length of the deposition region decreased (Fig. 4). The distance over which half of the deposition occurred normalized by the canopy height (/h) was longest for releases at the leading edge, where the vertical updraft was strongest, and shortened as the release points moved farther from the

leading edge and experienced weaker updrafts, until reaching the end of the adjustment zone, i.e.

(Table 2). The deposition region was shortest for the release at , because at this point the updraft was 0 (in Table 2) and the contribution from shear-layer vortices was still small, as reflected in the Reynolds stress value, which was smaller than in the fully developed region (, Fig. 3c).

The fraction of released particles ( ) that deposited to the bed (and were thus retained in the canopy) was calculated using eq. (3). was lowest for particles released at the leading edge, , and increased with distance from the leading edge for release points within the initial adjustment region, reaching a maximum at (Figure 5c). This was consistent with the expected influence of the updraft associated with the leading edge, which was maximum at the leading edge and decayed to zero at (Fig. 5a). The updraft carried particles out of the meadow, reducing deposition. Beyond , i.e. within the fully-developed region, decreased relative to peak at , due to increased turbulence in the upper canopy (Fig. 5b) associated with canopy scale vortices forming beyond . For all release locations, releases in the lower canopy (0.31) had greater deposition than releases in the upper canopy (0.81), because both the shorter distance to the bed and the significantly weaker turbulence near the bed were more favorable for deposition (Fig. 5b). It is likely that the fraction of mass that escaped the canopy ($1-F_{dep}$) was composed of the finer fraction of particles, as settling velocity decreases with particle diameter, reducing for the finer fraction, making them more easily transported out of the canopy by turbulence.

Finally, to examine the impact of settling velocity on particle deposition, two particle sizes ( ) were released in the fully developed region (Fig. 6). The release points were above and below the maximum penetration of the canopy scale vortices ( ), so that the canopy scale vortices routinely flushed the higher release point, while turbulence near the lower release point, dominated by stem scale vortices, was of lower intensity (Fig. 5b). The smaller particles (E3000) had a settling velocity about one order of magnitude less than the canopy shear velocity, so particle transport was expected to be influenced by canopy turbulence. Consistent with this, the smaller particles exhibited different retention when released in the upper canopy (higher turbulence) than in the lower canopy (lower turbulence) Specifically, for the smaller particles, a higher fraction deposited to the bed from the release at than the release at (Fig. 6, , , (SE),). In addition, deposition occurred over a shorter distance for the

release at than for the release at (m), respectively. In contrast, for the larger particles (A2024), was the same, within error, for the release at and the release at (Fig. 6, (SE), , ,). This is consistent with the expectation that the larger particles were not influenced by canopy turbulence.

Discussion

This experimental study demonstrated how flow adjustment at the leading edge of a submerged canopy impacts particle retention. Specifically, for a wide canopy of uniform frontal area density (as considered here), a vertical updraft at the leading edge diminished particle retention near the leading edge. Similarly, Cotton et al. (2006) observed that deposition began some distance beyond the leading edge of submerged canopies of water crowfoot. For narrow canopies, or near the lateral edge of a canopy, lateral flows are also generated near the leading edge, which may also carry particles out of the canopy before deposition is possible. For example, in an emergent canopy of finite width Zong and Nepf (2010) measured minimum deposition at the leading edge, and increasing deposition with distance from the leading edge. They attributed diminished deposition near the leading edge to both elevated turbulence in this region, as well as to flow deflection, which for their emergent canopy was lateral. In the field, canopies can be both submerged (height) and have finite width ( ), so that they may have both vertical and lateral flow deflection within the adjustment region. Such a three-dimensional flow diversion was observed around submerged circular patches of model flexible vegetation (Ortiz et al. 2013). The relative magnitude of the vertical and lateral flow deflections depends on the aspect ratio of the patch. Wide patches ( ) deflect flow vertically, while flow around narrower patches ( ) would be dominated by lateral deflection. Both lateral and vertical deflection can carry particles out of a meadow, diminishing deposition within the leading edge.

It is important to note that vertical variation in frontal area density may alter the pattern of flow deflection, changing the impact on particle fate. For example, Pan et al. (2015) numerically modeled particle transport within a corn canopy with frontal area density that varied with vertical position. The densest region of the canopy was between 0.3 and 0.9 (2.1 m, 0.8). At the leading edge, the flow diverged around the high-density zone, producing an updraft in the upper canopy (0.66) and a downdraft in the lower canopy (

0.33). Because the downdraft pushed particles towards the bed, the fraction of particles captured was elevated at the leading edge ( ) of the corn canopy, which is opposite to the trend we observed for a model with uniform frontal area. Further, in the corn canopy, particle retention reached a minimum after the downdraft decayed ( ). Beyond this point, particle capture within the modeled corn canopy increased as the vertical updraft in the upper canopy decayed ( ).

The effect of flow structure, including the diversion within the adjustment region at the leading edge, should be considered when designing experimental studies in submerged canopies. Based on field observations on Zostera marina canopies, we can estimate the expected range of the adjustment length-scales, . McKone (2009) reported the leaf area index (, 3.95, 2.46, respectively), which we assumed to equal *ah*. Using C_D = 1,eq. 2 predicts 8.1, 9.7, 7.7, respectively. Moore (2004) measured the biomass in seagrass beds in the Lower Chesapeake Bay, which could be converted to area density by dividing by the material density of the seagrass, kg m^{-3} (Fonseca 1998) and blade thickness mm (——— , Luhar et al. 2008), resulting in 0.4 – 1 (Luhar et al., 2008) and 14.4 – 9.9, respectively. Based on these estimates, the adjustment length for typical *Zostera marina* meadows is approximately 10*h*, suggesting that the deposition pattern within the first 10*h* distance along a meadow will be different from that in the fully developed region beyond 10*h*. In patchy landscapes, for which the length of the canopy is less than , flow diversion would occur over the full patch length, suggesting that patchy seagrass meadows would have reduced particle retention, relative to a contiguous meadow of the same total area. However, distance between meadows is also important. For example, Folkard showed that flow in gaps < 1.75 displayed little to no change from in-canopy flow (Folkard 2005, 2011), so that patchy meadows with small gaps may act as a continuous canopy. During meadow decline, seagrass canopies have been observed to degrade from a single large canopy to a patchy landscape (Jill Carr, personal communication, March 30, 2016). Establishment of such a patchy pattern could reduce sediment deposition and enhance resuspension, with these negative feedbacks further contributing to meadow decline**.**

Tidal current variations and wave motion also influence particle behavior in the field. Changes in tidal current would create varying , resulting in changing particle transport behavior, which is controlled by Near slack tide, when , all particles within a meadow would tend to settle within the meadow, but with no mean current, no new particles would be supplied to the meadow. As flow accelerates, velocity over the bare bed

may increase enough to resuspend particles that may be supplied to the meadow, but retention in the meadow would depend on the meadow length and canopy turbulence, as described above. Since the canopy shear velocity increases with current speed (, Ghisalberti 2009), within a tidal cycle, particles of a particular size (particular w_s) may transition from being likely to deposit within a meadow ( ) to being unlikely to deposit within a meadow ( ). Wave oscillatory velocities experience less attenuation within submerged canopies, compared to unidirectional currents (Lowe et al. 2005; Luhar et al. 2010), so that wave-dominated conditions do not create strong gradients in velocity near canopy edges, which in turn would lead to more uniform deposition patterns within the meadow.

Conclusion

Submerged aquatic vegetation creates a complex flow structure that influences the fate of particles within the canopy. At the leading edge flow is deflected away from the region of high drag, and in a wide meadow , this creates a vertical updraft within the adjustment region. If particle settling velocity is comparable to or less than the updraft magnitude, then particle capture will be diminished by the presence of the updraft. Because the updraft decays with distance from the leading edge, particle retention increases with distance from the leading edge, reaching a maximum at the end of the adjustment region (, where the updraft has fully decayed, and the canopy scale vortices are still small. In the fully-developed region, particles below the region flushed by canopy scale vortices have higher retention than particles within the upper canopy . Because particle retention is diminished near the leading edge, estimates of meadow-scale particle retention should consider the spatial variation across this region, especially when is comparable to meadow size.

Acknowledgements:

This material is based upon work supported by the National Science Foundation under Grant No. AGS-1005480. Any opinions, findings, or recommendations expressed in this material are those of the authors and do not necessarily reflect the views of the National Science Foundation.

References

Agawin, N.S.R., and G.M. Duarte. 2002. Evidence of direct particle trapping by a tropical seagrass meadow. *Estuaries and Coasts* 25: 1205–1209.

Belcher, S.E., Jerram, N., and J.C.R. Hunt. 2003. Adjustment of a turbulent boundary layer to a canopy of roughnesss elements. *Journal of Fluid Mechanics* 488: 369–398.

Chen, Z., Ortiz, A., Zong, L., and H. Nepf. 2012. The wake structure behind a porous obstruction and its implications for deposition near a finite patch of emergent vegetation. *Water Resources Research* 48: W09517. doi:10.1029/2012WR012224.

Chen, Z., Jiang, C., and H. Nepf. 2013. Flow adjustment at the leading edge of a submerged aquatic canopy. *Water Resources Research* 49: 5537-5551. doi:10.1002/wrcr.20403.

Cotton, J.A., Wharton, G., Bass, J.A.B., Heppell, C.M., and R.S. Wotton. 2006. The effects of seasonal changes to in-stream vegetation cover on patterns of flow and accumulation of sediment. *Geomorphology* 77: 320–334.

Folkard, A. 2005. Hydrodynamics of model *Posidonia oceanica* patches in shallow water. *Limnology and Oceanography* 50: 1592–1600.

Folkard, A. 2011. Flow regimes in gaps within stands of flexible vegetation: laboratory flume simulations. *Environmental Fluid Mechanics* 11, 289–306.

Gacia, E., and C.M. Duarte. 2001. Sediment retention by a Mediterranean *Posidonia oceanica* meadow: the balance between deposition and resuspension. *Estuarine, Coastal, and Shelf* Science 52: 505–514.

Gacia, E., Granata, T.C., and C.M. Duarte. 1999. An approach to the measurement of particle flux and sediment retention within seagrass (*Posidonia oceanica*) meadows. *Aquatic Botany* 65: 255–268.

Ghisalberti, M., and H. Nepf. 2002. Mixing layers and coherent structures in vegetated aquatic flows. *Journal of Geophysical Research* 107: 3011.

Ghisalberti, M., and H. Nepf. 2004. The limited growth of vegetated shear layers. *Water Resources Research* 40: W07502. doi: 10.1029/2003WR002776.

Green, E.P., and F.T. Short. 2003. *World Atlas of Seagrasses*. Oakland: University of California Press.

Gurnell, A.M., Petts, G.E., Hannah, D.M., Smith, B.P.G., Edwards, P.J., Kollmann, J., Ward, J.V., and K. Tockner. 2001. Riparian vegetation and island formation along the gravel-bed Fiume Tagliamento, Italy. *Earth Surface Processes and Landforms* 26: 31–62.

Hughes, A.R., and J.J. Stachowicz. 2004. Genetic diversity enhances the resistance of a seagrass ecosystem to disturbance. *Proceedings of the National Academy of Sciences* 101: 8998–9002.

Irvine, M., Gardiner, B., and M. Hill. 1997. The evolution of turbulence across a forest edge. *Boundary Layer Meteorology* 84: 467-496.

van Katwijk, M.M., Bos, A.R., Hermus, D.C.R., and W. Suykerbuyk. 2010. Sediment modification by seagrass beds: Muddification and sandification induced by plant cover and environmental conditions. *Estuarine, Coastal and Shelf Science* 89: 175–181.

van Katwijk, M., Thorhaug, A., Núria, M., Orth, R., Duarte, C., Kendrick, G., … and J. Verduin. 2016. Global analysis of seagrass restoration: the importance of large-scale planting. *Journal of Applied Ecology* 53: 567–578.

Lamb, J.B., van de Water, J.A.J.M., Bourne, D.G., Altier, C., Hein, M.Y., Fiorenza, E.A., Abu, N., Jompa, J., Harvell, C.D., 2017. Seagrass ecosystems reduce exposure to bacterial pathogens of humans, fishes, and invertebrates. *Science* 355: 731-733.

Lawson, S.E., McGlatherty, K.J., and P.L. Wiberg. 2012. Enhancement of sediment suspension and nutrient flux by benthic macrophytes at low biomass. *Marine Ecology Progress Series* 448: 259–270.

Luhar, M., Rominger, J., and H. Nepf. 2008. Interaction between flow, transport, and vegetation spatial structure. *Environmental Fluid Mechanics* 8: 423–439.

Liu, C., and H. Nepf. 2016. Sediment deposition within and around a finite patch of model vegetation over a range of channel velocity. *Water Resources Research* 51(1):600-612*,* doi:10.1002/2015WR018249

Marbà, N., Arias-Ortiz, A., Masqué, P., Kendrick, G.A., Mazarrasa, I., Bastyan, G.R., Garcia-Orellana, J., and C.M., Duarte. 2015. Impact of seagrass loss and subsequent revegetation on carbon sequestration and stocks. *Journal of Ecology* 103, 296–302. McKone. K., 2009. Light available to the seagrass *Zostera marina* when exposed to currents and waves. *University of Maryland, Ph.D. thesis*.

Moore, K.A. 2004. Influence of seagrasses on water quality in shallow regions of the lower Chesapeake Bay. *Journal of Coastal Research* 20: 162–178.

Morse, A., Gardiner, B., and B. Marshall. 2002. Mechanisms controlling turbulence development across a forest edge. *Boundary Layer Meteorology* 103: 227–251.

Nepf, H., and E.R. Vivoni. 2000. Flow structure in depth-limited, vegetated flow. *Journal of Geophysical Research* 105: 28547–28557.

Nepf, H., Ghisalberti, M., White, B, and E. Murphy. 2007. Retention time and dispersion associated with submerged aquatic canopies. *Water Resources Research* 43: W04422.

Ortiz, A.C., Ashton, A., and H. Nepf. 2013. Mean and turbulent velocity fields near rigid and flexible plants and the implications for deposition. *Journal of Geophysical Research: Earth Surface* 118: 2585–2599

Pan, Y., Chamecki, M., Isard, S.A., and H. Nepf. 2015. Dispersion of particles released at the leading edge of a crop canopy. *Agricultural and Forest Meteorology* 211-212: 37–47.

Poindexter, C.M., Rusello, P.J., and E.A. Variano. 2011. Acoustic Doppler velocimeter-induced acoustic streaming and its implications for measurement. *Experiments in Fluids* 50: 1429–1442.

Raupach, M.R., Finnigan, J.J., and Y. Brunet. 1996. Coherent eddies and turbulence in vegetation canopies: the mixing-layer analogy. *Boundary-Layer Meteorology 25th anniversary volume, 1970-1995*: 351–382.

Sand-Jensen, K. 1998. Influence of submerged macrophytes on sediment composition and near-bed flow in lowland streams. *Freshwater Biology* 39: 663–679.

Tanaka, N., and J. Yagisawa. 2010. Flow structures and sedimentation characteristics around clump-type vegetation, *Journal of Hydro-environment Research* 4: 15–25. doi:10.1016/j.jher.2009.11.002.

Terrados, J., and C.M. Duarte. 2000. Experimental evidence of reduced particle resuspension within a seagrass (*Posidonia oceanica*) meadow. *Journal of Experimental Marine Biology and Ecology* 243: 45–53.

Ward, L.G., Kemp, W.M., and W.R. Boynton. 1984. The influence of waves and seagrass communities on suspended particulates in an estuarine embayment. *Marine Geology 59*: 85–103.

Waycott, M., Duarte, C., Carruthers, T., Orth, R., Dennison, W., Olyarnik, S., Calladine, A., Fourqurean, J., Heck, K., Hughes, A.R., Kendrick, G., Kenworthy, W.J., Short, F., Williams, S., 2009. Accelerating loss of seagrasses across the globe threatens ecosystems. *Proceedings of the National Academy of Sciences* 106: 12377-12381.

Zong, L., and H. Nepf. 2010. Flow and deposition in and around a finite patch of vegetation. *Geomorphology* 116: 363–372.

Figure Captions

Figure 1 Schematic of flow adjustment from flow over a bare bed to flow over submerged vegetation, showing, canopy height , and canopy length . Flow depth is H. Flow decelerates starting at , creating an updraft over length . A mixing layer grows and becomes fully developed at , after which point friction velocity at canopy height ( ) has a constant value. Characteristic vortex penetration in this fully developed region is .

Figure 2 Schematic of slide and canopy element locations between 42 and 65) for release within the fully developed region at (black star). Deposited particles were captured on glass microscope slides, represented by gray rectangles. Canopy elements are represented by black dots; flow direction is shown by a black arrow.

Figure 3 Contour plots in vs. plane showing (a) time-averaged longitudinal velocity (m s^{-1}), (2) time-averaged vertical velocity (m s^{-1}), and (c) Reynolds stresses (m^2 s^{-2}) from data collected at 1, 0.81, and 0.31 and at 43 positions in streamwise direction . Initial adjustment length, , is shown with a solid vertical line. Data collected after were smoothed with a 5-point running average, to remove fluctuations associated with canopy heterogeneity. The fully-developed region begins at , which is shown with a dashed vertical line. The penetration distance of canopy scale vortices, 0.43.

Figure 4 Longitudinal ( ) deposition patterns (g cm^{-2}) created by injections made at nine locations inside the canopy. Silica particles (m s^{-1}) were released at (a) , and (b) . Dashed vertical lines indicate the longitudinal positions of individual particle releases. Solid vertical line denotes position of .

Figure 5 Longitudinal profile of (a) vertical velocity and (b) turbulent kinetic energy at two vertical positions (0.31, 0.81, black and grey solid circles), and (c) fraction of released particles ( ) that deposited to bed for two release heights (, black triangles; , gray triangles). Vertical lines on points at 0, 53.3 denote difference between two replicates at these positions. Standard error at 0 and 53.3 was $(SE)^{-}$ = 0.013 and 0.03, respectively. We assume these are also representative of the error at 2.4, 5, 13.7. The error is comparable to the size of the symbol shown.

Figure 6 Deposition (g cm^{-2}) of silica particles in two sizes: (a) (E3000) and (b) (A2024) injected within the canopy fully developed region (53.3). Particles were injected above (, solid circles), in the region routinely flushed by canopy scale vortices, and below (, open circles), in the region characterized by stem-scale vortices.

Table Captions

Table 1 Diameter and settling velocities of smaller (E3000) and larger (A2024) particles. Values shown for 10, 25, 50, 75, and 90th percentiles. Particle size distribution measured using laser diffraction (Beckman Coulter).

Table 2 Updraft ( ) at release point, distance over which half of total deposition occurred ( ), distance between release and the point of maximum deposition ( ), and the fraction of released particles that deposited to the bed for releases of spherical silica particles ( ) at (a) , and (b) . Standard error reported in table for and was found from replicate experiments at 0 and 53.3. Release point , indicated by an asterisk, is closest to .

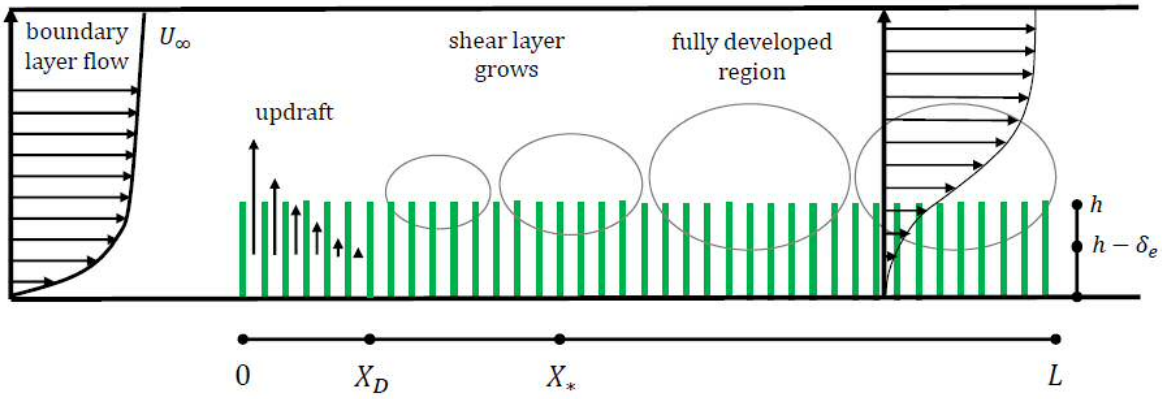
boundary
layer flow
U_∞
updraft
shear layer
grows
fully developed
region
h
$h - \delta_e$
0
X_D
X_*
L

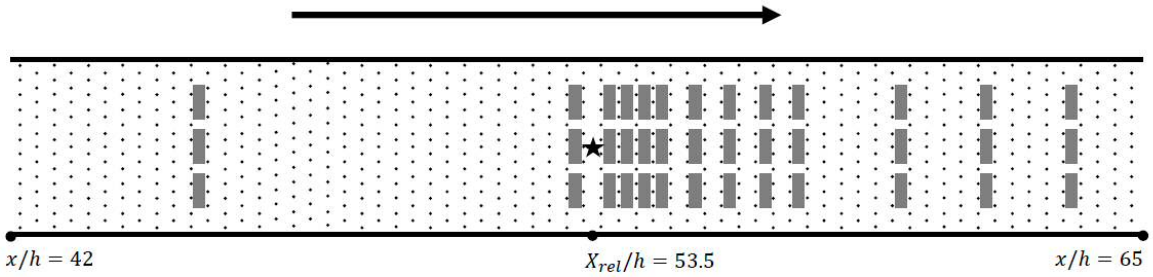
$x/h = 42$
$X_{rel}/h = 53.5$
$x/h = 65$

Figure 3

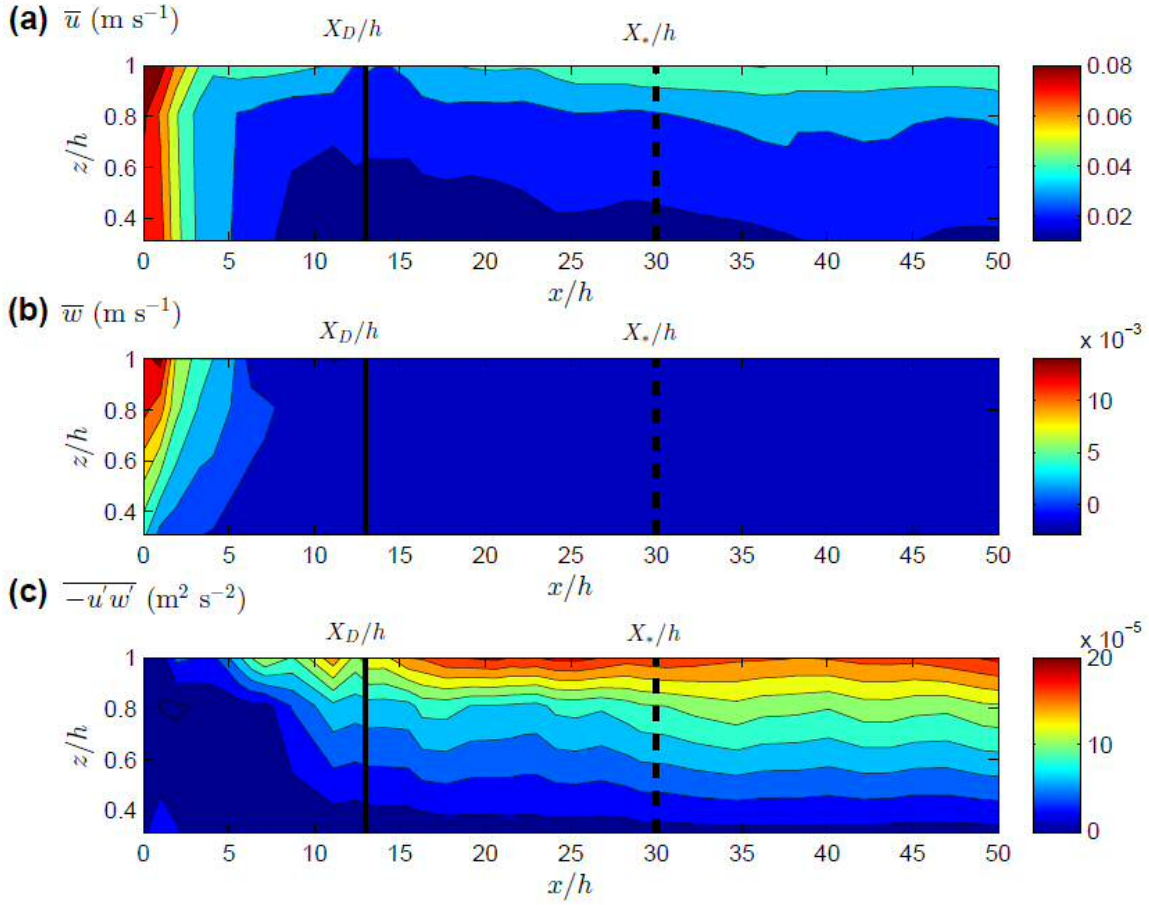
(a) $\overline{u}$ (m s^{-1})
X_D/h
X_*/h
z/h
x/h
0.08
0.06
0.04
0.02
(b) $\overline{w}$ (m s^{-1})
x 10^{-3}
10
5
0
(c) $\overline{-u'w'}$ (m^2 s^{-2})
x 10^{-5}
20
10
0

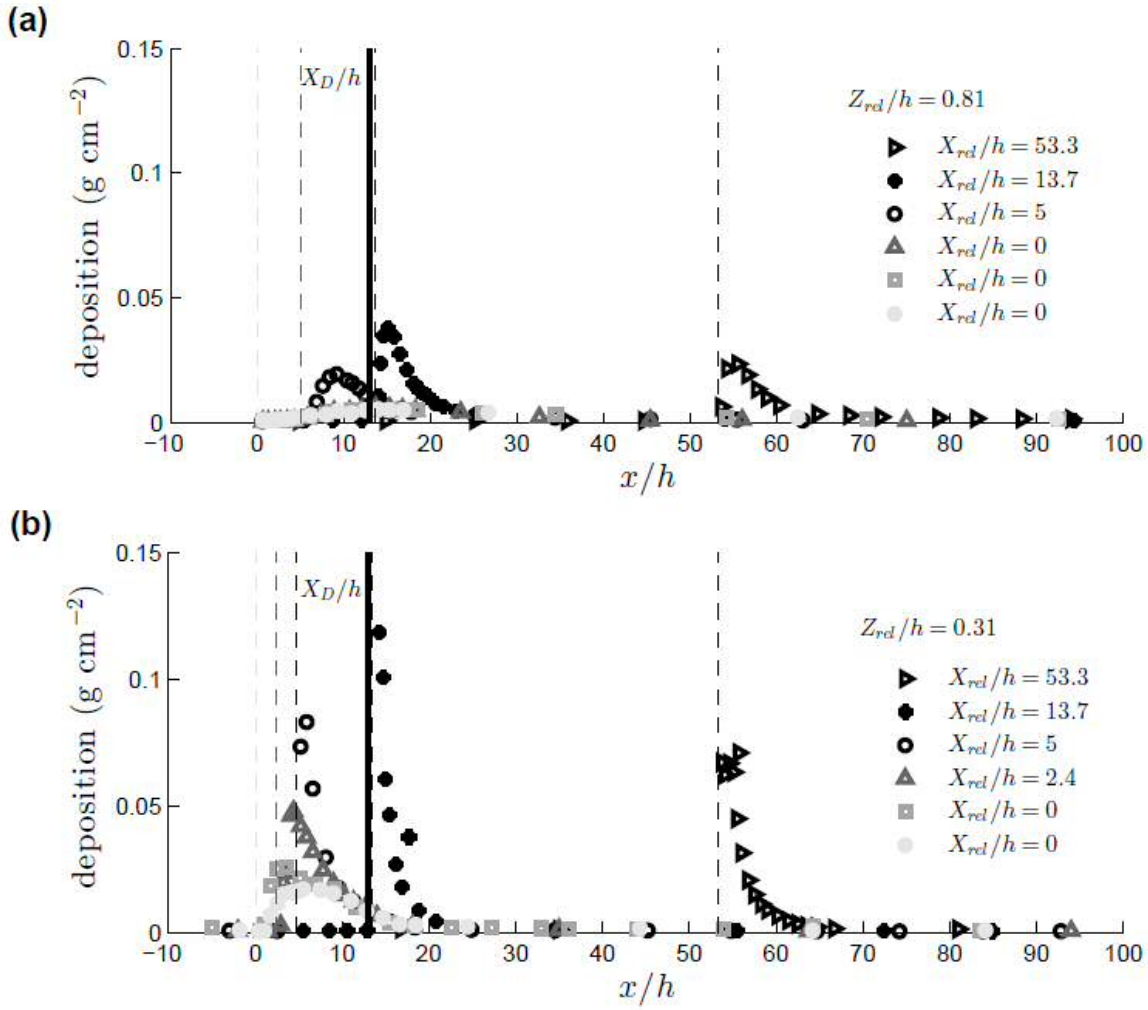
(a)
deposition (g cm^{-2})
X_D/h
$Z_{rd}/h = 0.81$
$X_{rd}/h = 53.3$
$X_{rd}/h = 13.7$
$X_{rd}/h = 5$
$X_{rd}/h = 0$
$X_{rd}/h = 0$
$X_{rd}/h = 0$
x/h
(b)
deposition (g cm^{-2})
X_D/h
$Z_{rd}/h = 0.31$
$X_{rd}/h = 53.3$
$X_{rd}/h = 13.7$
$X_{rd}/h = 5$
$X_{rd}/h = 2.4$
$X_{rd}/h = 0$
$X_{rd}/h = 0$
x/h

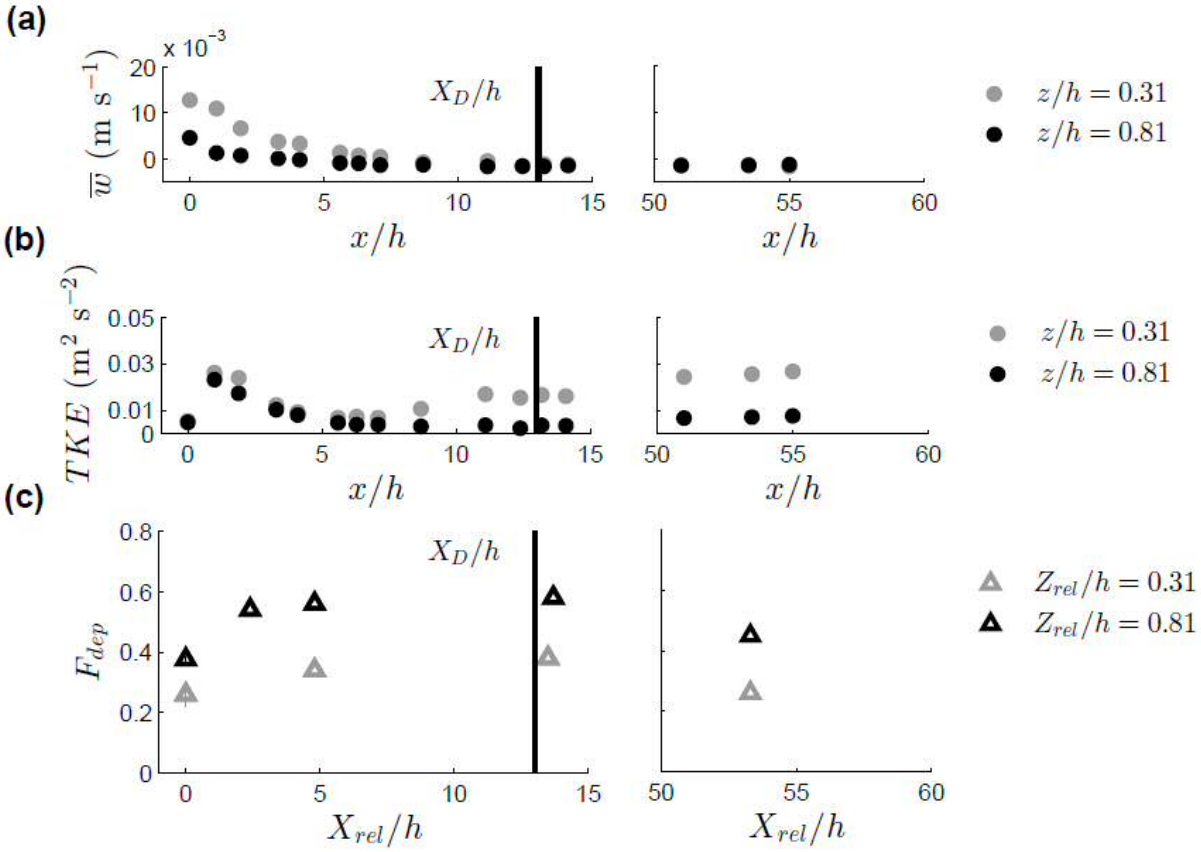
(a)
x 10^-3
20
10
0
$\overline{w}$ (m s^{-1})
X_D/h
0
5
10
15
50
55
60
x/h
x/h
$z/h = 0.31$
$z/h = 0.81$
(b)
0.05
0.03
0.01
0
TKE (m^2 s^{-2})
X_D/h
x/h
x/h
$z/h = 0.31$
$z/h = 0.81$
(c)
0.8
0.6
0.4
0.2
0
F_{dep}
X_D/h
X_{rel}/h
X_{rel}/h
$Z_{rel}/h = 0.31$
$Z_{rel}/h = 0.81$

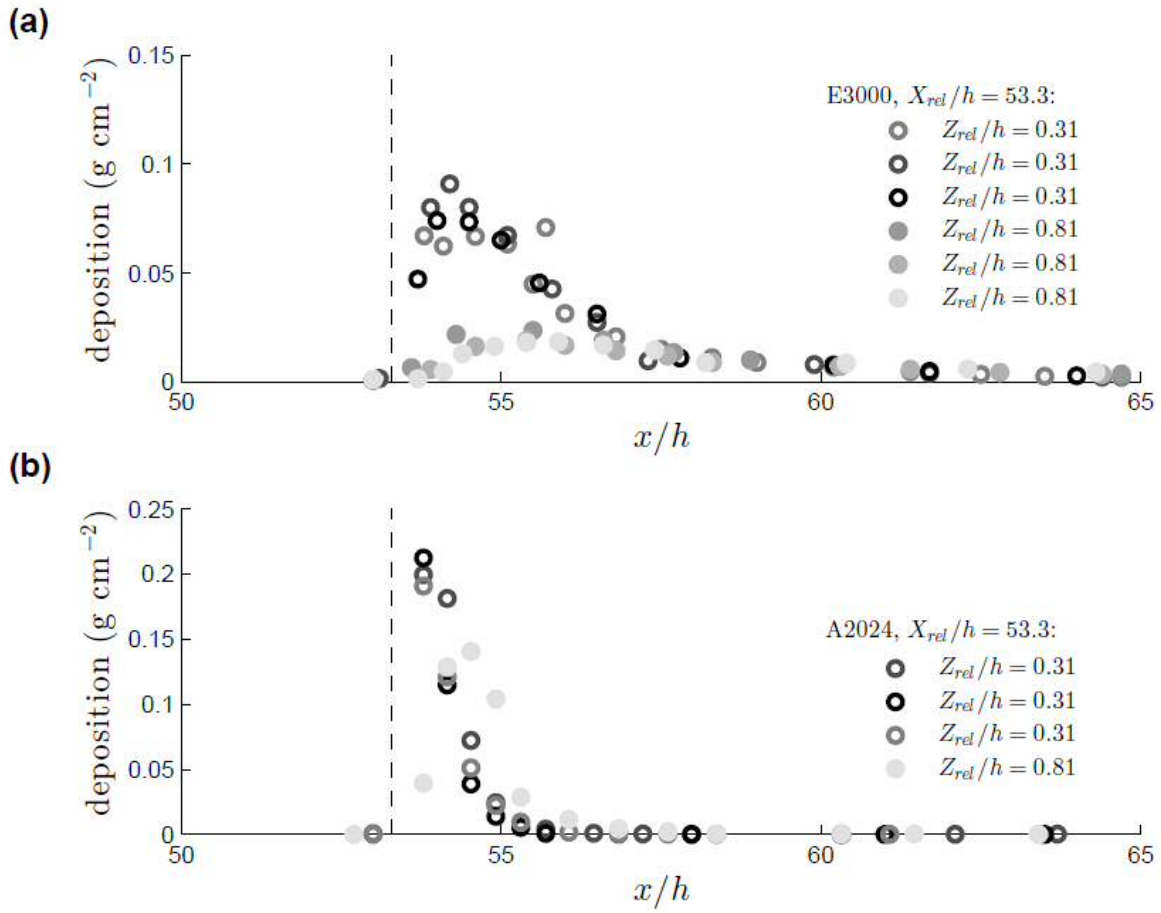

E3000:	%	*d* (*μ*m)	w_s (m s^{-1})	A2024:	%	*d* (*μ*m)	w_s (m s^{-1})
	10	4.8	2.1 x 10^{-5}		10	130	1.5 x 10^{-2}
	25	13	1.6 x 10^{-4}		25	140	1.6 x 10^{-2}
	50	29	7.5 x 10^{-4}		50	150	1.8 x 10^{-2}
	75	50.	2.3 x 10^{-3}		75	170	2.1 x 10^{-2}
	90	77	5.4 x 10^{-3}		90	180	2.2 x 10^{-2}

(a)					
Z_{rel}/h=0.81					
X_{rel}/h	0	5	13.7*	53.3	
$\overline{w}$ m s^{-1}	0.0128	0.0022	-0.0010	-0.0004	
$X_{1/2}$m	2.5 ± 0.4	0.78	0.39	0.54 ± 0.07	
L_{max} m	1.5 ± 0.1	0.42	0.14	0.23 ± 0.03	
F_{dep}	0.26 ± 0.04	0.34	0.38	0.26 ± 0.02	
(b)					
Z_{rel}/h=0.31					
X_{rel}/h	0	2.4	5	13.7*	53.3
$\overline{w}$ m s^{-1}	0.0046	0.0005	-0.0006	-0.0015	-0.0015
$X_{1/2}$m	0.80 ± 0.1	0.47	0.23	0.15	0.19 ± 0.01
L_{max} m	0.50 ± 0.1	0.2	0.11	0.03	0.12 ± 0.09
F_{dep}	0.376 ± 0.006	0.54	0.56	0.58	0.45 ± 0.02